# Band-gap engineering of $Zn_{1-x}Ga_xO$ nanopowders: Synthesis, structural and optical characterizations

Michael Snure and Ashutosh Tiwari[a)]
*Nanostructured Materials Research Laboratory, Department of Materials Science and Engineering, University of Utah, Salt Lake City, Utah 84112, USA*

(Received 20 June 2008; accepted 8 August 2008; published online 2 October 2008)

We report the preparation and detailed structural and optical characterizations of single phase gallium doped ZnO nanopowders. A low temperature solution-based technique was developed to synthesize high-purity $Zn_{1-x}Ga_xO$ ($x$:0–0.05) nanopowders. Structural and optical characterization experiments were performed using x-ray diffraction (XRD), energy dispersive x-ray spectroscopy, scanning electron microscopy, photoluminescence spectroscopy, Raman spectroscopy, and optical transmission spectroscopy. Analysis of XRD data showed a maximum in the lattice volume for $x=0.03$ as the Ga concentration increases in the $Zn_{1-x}Ga_xO$ series. Optical transmission spectroscopy results also showed an initial increase in the band gap ($E_g$) followed by a decrease for $x>0.04$. A maximum band gap was observed for the $Zn_{0.96}Ga_{0.04}O$ sample, which has a value of 3.42 eV compared to the band-gap value of 3.31 eV for the undoped ZnO sample. All $Zn_{1-x}Ga_xO$ nanopowder samples showed a broad photoluminescence spectrum with significant shift in peak positions compared to bulk ZnO sample. The broadening and shifting in luminescence are understood to be caused by the nanocrystalline nature of the material and the presence of deep-level surface defects. These effects were further investigated by Raman microscopy where an increase in the intensity of $E_1$(TO) mode was observed accompanied by the appearance of a few additional Raman active modes. © *2008 American Institute of Physics*. [DOI: 10.1063/1.2988131]

## I. INTRODUCTION

In the past few years much scientific attention has been focused on finding good transparent conducting oxides for a wide number of applications. ZnO holds a special place among these materials because of its good optical properties and ability to increase conductivity with increased oxygen vacancies.[1–8] *N*-type doping of ZnO with group IIIB elements such as Al, Ga, and In has also been shown to greatly increase conductivity while maintaining good optical transparency.[1] Moreover, the large band gap (3.3 eV) and high exciton binding energy (60 meV) of ZnO result in high luminescent efficiencies. It has been shown that the band gap of ZnO thin films can be tuned by adding dopants. For instance $E_g$ can be increased by alloying with materials such as MgO (8.2 eV) and decreased by alloying with CdO (2.0 eV).[2,3] In addition to this, $E_g$ can also be tuned by introducing strain and point defects.[4,5] The above properties of ZnO are indeed much superior to GaN, the other most widely used wide band-gap semiconductor, which has a band gap of 3.44 eV and exciton binding energy (26 meV) that is only slightly above the thermal energy at room temperature.[6,7]

Many of zinc oxide's properties show considerable enhancement as dimensions are decreased to the nanometer scale. Because of this, many different low-dimensional structures such as thin films, nanorods, nanoscrews, and nanobelts have been grown by a number of different techniques in the past.[9,10] However, most of these techniques require high temperatures and high vacuum. So, recently a significant amount of effort has also been focused on developing low temperature solution based methods for growing these nanostructures. Recently, we have developed a citrate-precursor based sol-gel technique for synthesizing ZnO-based nanostructures.[11] Our method allows us to produce large quantities of uniformly doped nanostructured materials at significantly lower temperatures than used in solid-state methods. In this paper we are presenting our results on the synthesis and structural and optical characterizations of $Zn_{1-x}Ga_xO$ nanopowders.

## II. EXPERIMENTAL PROCEDURE

Starting materials used in our processing technique were ZnO (99.9% metal basis, 5 $\mu$m in diameter) and $Ga_2O_3$ (99.99% metal basis, 75 $\mu$m in diameter). ZnO was dissolved in concentrated nitric acid ($HNO_3$) at room temperature and $Ga_2O_3$ in a heated 1 M sodium hydroxide (NaOH) solution. These two solutions were mixed in stoichiometric amounts to get the desired composition $Zn_{1-x}Ga_xO$ ($x=0.01–0.05$). The combined solution was heated until the solution became clear. Citric acid was then dissolved in water and added to the solution in such amount that the ratio of metal ions ($Zn^{2+}$ and $Ga^{3+}$) to citric acid was 1:1. Citric acid in this solution acts as a chelating agent that binds the metallic ions in solution to the acid carbon chain.[11] The transparent homogeneous solution thus obtained was refluxed for 12 h using a condenser to maintain the starting volume of the solution. Once the refluxing was complete the solution was heated and allowed to reduce to a gel. This gel was further heated until a highly exothermic reaction took place producing highly porous nanostructured powders. A differential

a)Author to whom correspondence should be addressed. Electronic mail: tiwari@eng.utah.edu.

 

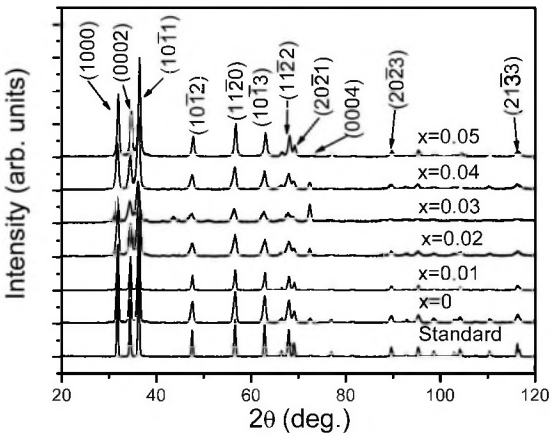


FIG. 1. $\theta$-$2\theta$ XRD pattern of the $Zn_{1-x}Ga_xO$ ($x$=0–0.05) nanopowders. For comparison we have also shown the XRD data for the coarse ZnO precursor powder.

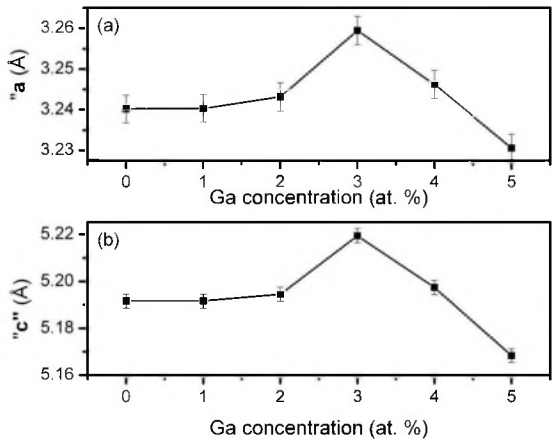


FIG. 2. (a) Lattice parameter $a$ of $Zn_{1-x}Ga_xO$ as a function of Ga concentration. (b) Lattice parameter $c$ of $Zn_{1-x}Ga_xO$ as a function of Ga concentration.

scanning calorimeter measurement showed that the gel to powder reaction took place at a temperature below 160 °C. The nanostructured powders were then heated in a furnace from room temperature to 500 °C at the rate of 10 °C per minute and then held at 500 °C for 1 h to remove any remaining carbon. The powders were then cooled at a rate of 10 °C per minute to room temperature.

The $Zn_{1-x}Ga_xO$ ($x$=0–0.05) samples prepared in this study were characterized using energy dispersive x-ray spectroscopy (EDS), x-ray diffraction (XRD), scanning electron microscopy (SEM), photoluminescence spectroscopy (PL), Raman spectroscopy, and optical transmission spectroscopy. The SEM and EDS measurements were performed using a Hitachi S3000-N scanning electron microscope with an EDAX S3000-N detector. XRD scans were done using a Phillips X'pert diffractometer with copper $K\alpha$ x-ray source and nickel filter. Raman spectroscopy measurements were performed at room temperature by exciting the samples with a laser power of 120–140 mW in the backscattering geometry with the 514.5 nm (2.41 eV) line of an argon ion laser using an ISA U-1000 scanning double monochromator (Jobin Yvon, USA). Care was taken to ensure that the excitation laser did not cause the heating of the sample. Optical transmittance measurements were performed using a DU 730 UV/visible scanning spectrophotometer in wavelength scanning mode. Samples for optical transmittance measurements were prepared by combining 1 mg of sample with 300 mg of potassium bromide (KBr) and pressing them into a pellet. The KBr was kept under vacuum to avoid water absorption. PL measurements were made using a JY spectrometer with a thermoelectrically cooled charge coupled device detector. Excitation of samples was done using the 325 nm (20 mW) line of a He–Cd laser (Kimmon Electric).

## III. RESULTS AND DISCUSSION

Figure 1 shows $\theta$-$2\theta$ XRD patterns for $Zn_{1-x}Ga_xO$ ($x$=0–0.05) nanopowders prepared in this study. For comparison we have also shown the XRD pattern of the coarse ZnO precursor in this figure. All the $Zn_{1-x}Ga_xO$ XRD patterns match very well with the diffraction pattern for the hexagonal wurtzite ZnO precursor. No additional peaks could be detected in these patterns, implying the high phase purity of the material. As can be seen in Fig. 1, there is quite significant broadening in the diffraction peaks of $Zn_{1-x}Ga_xO$ compared to the ZnO precursor sample. The broadening in the diffraction peaks of sol-gel prepared samples is understood to arise because of the reduction in the crystallite size, which was calculated using Scherrer's formula[12] to be 26, 28, 20, 17, 15, and 23 nm for x=0, 0.01, 0.02, 0.03, 0.04, and 0.05, respectively. For the Ga doped samples we also saw a slight shift in the positions of the first three peaks. These peak shifts appear to be caused by the changes in lattice parameters $a$ and $c$. Figure 2 shows how both $a$ and $c$ change as a function of Ga doping. Lattice parameter $a$ was calculated from (10$\bar{1}$0) and (20$\bar{2}$0) peaks and $c$ from (0002) and (0004) peaks. In Fig. 2 we see that both $a$ and $c$ initially increased until a maximum (3.26 Å for $a$ and 5.22 Å for $c$) was reached at 3% Ga doping. The lattice parameters then decrease as the percent of Ga doping further increases to 5%. At 5% Ga doping lattice parameters $a$ and $c$ were 3.23 and 5.22 Å, respectively.

Variation in the lattice parameters and hence in the lattice volume is understood to arise because of two competing factors: (i) a size difference between the ionic radii of $Zn^{2+}$ (0.74 Å) and $Ga^{3+}$ (0.62 Å) and (ii) deformation of the conduction band potential caused by an increase in free carriers.[13,14] As Ga is doped into ZnO because of the dominant 3+ ionic nature of Ga ions, electrons are introduced into the system. Now since the material is extremely porous with nanocrystallites separated by highly resistive grain boundaries, electrons have to remain confined inside the nanocrystals. A high concentration of confined electrons results in an increase in the Coulomb repulsion energy. So in order to minimize the overall energy of the system, lattice expands. This results in an increase in the lattice volume as observed in Fig. 2. However, when more Ga are substituted into the ZnO system the difference in ionic radii of $Zn^{2+}$ and $Ga^{3+}$ starts playing an increasingly important role causing the volume of the unit cell to decrease.

Figure 3 shows EDS scans for the $Zn_{1-x}Ga_xO$ samples. Only peaks corresponding to Zn ($L\beta$, $K\alpha$, $K\beta$), O ($K\alpha$), and

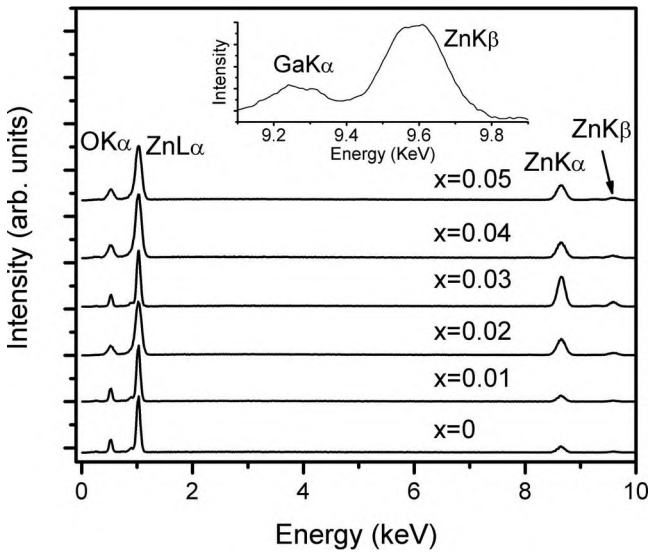


FIG. 3. EDS scans for the $Zn_{1-x}Ga_xO$ nanopowders. The inset shows the close-up of the $x=0.05$ sample over the energy range of 9.0–10.0 keV.

Ga ($K\alpha$) are detected. This indicates that the samples are free of contamination and reinforces the XRD results that indicated the high phase purity of sol-gel prepared $Zn_{1-x}Ga_xO$ samples. Figure 4 shows a SEM image of the highly porous nanostructured powders. Features such as walls with dimensions ranging from a few hundred nanometers to less then 100 nm can clearly be seen throughout the powders. From XRD data, the particle size was estimated to be between 17 and 28 nm. This suggests that the walls are actually made up of smaller agglomerated particles held together by high surface charges and are not solid walls made of a single particle.

The photoluminescence spectra of the $Zn_{1-x}Ga_xO$ samples along with the precursor ZnO are shown in Fig. 5. It is generally observed that ZnO exhibits three PL emission bands, a UV peak, a green peak, and a red peak. The UV peak occurs at about 380 nm and is due to the free-electron emission between the exciton and valance bands. The green and red bands occur at ~510 and ~650 nm, respectively, and are understood to be caused by deep level defects in the band. These deep level defects responsible for emission bands in the visible portion of the spectrum result from the oxygen vacancies, zinc vacancies, zinc interstitial ions, and crystal defects.[15,16]

As can be seen in Fig. 5 the PL spectra for the precursor ZnO sample show only one sharp peak centered at 391 nm,

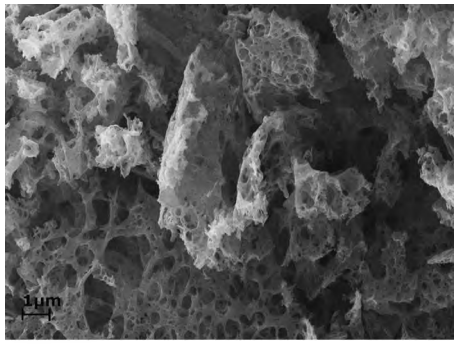


FIG. 4. SEM image of nanostructured $Zn_{0.99}Ga_{0.01}O$ nanopowder.

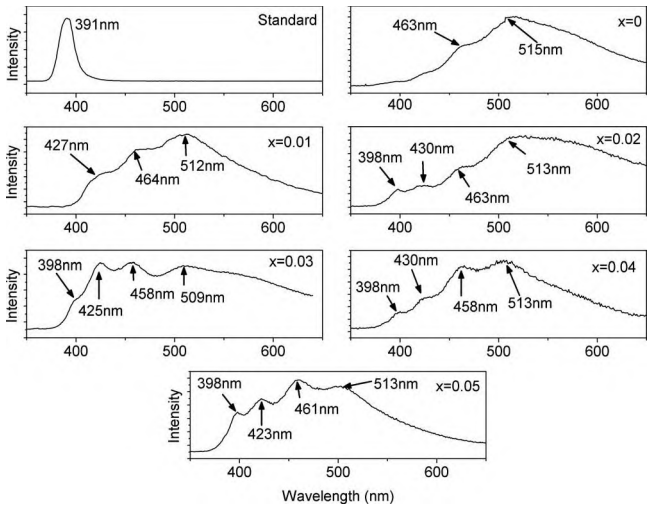


FIG. 5. PL spectrum for the $Zn_{1-x}Ga_xO$ nanopowders. For comparison we have also shown the PL data for the coarse ZnO precursor powder.

which is characteristic of highly crystalline ZnO. In contrast to this, $Zn_{1-x}Ga_xO$ samples show very broad peaks with luminescence in the visible spectrum. The luminescence peak of pure ZnO nanopowder sample has shifted to ~515 nm (a green peak) and displays a shoulder at 463 nm, implying that the sample has many deep level traps caused by the introduction of crystallographic and chemical defects. These effects are quite expected because of the highly porous nanocrystalline nature of the material. In the Ga doped samples we saw the formation of new emission peaks, violet and blue, as the concentration of Ga increases in the system. In addition to above the reappearance of the UV peak was also noticed. However, the UV peak was slightly redshifted to ~396 nm compared to 391 nm for the precursor ZnO sample. We believe that the onset of violet peak is caused by the creation of a donor band, which lies just below the conduction band of ZnO. As the amount of Ga in the system is increased, the blue peak replaces the green peak as the most intense luminescence peak. This means that the formation of the blue peak caused by a new impurity band is directly related to the concentration of Ga substituted into the system.

Figure 6 shows the optical transmittance of the $Zn_{1-x}Ga_xO$ samples as a function of wavelength. Due to the increased scattering caused by the particles being suspended in a KBr pellet, the absolute transmittance could not be determined. However, it can clearly be seen that there is a blueshift in the optical absorption edge as Ga concentration increases. Energy gaps ($E_g$) for the precursor and 0%–5% Ga doped samples were obtained by plotting $\alpha^2$ versus $h\nu$ ($\alpha$ is absorption coefficient and $h\nu$ is photon energy) and extrapolating the straight-line portion of the plot to zero. The inset of Fig. 6 shows a plot of $E_g$ with Ga concentration. Initially $E_g$ increases with increase in Ga concentration until a maximum (3.45 eV) is reached at a Ga concentration of 4%. Beyond this point, if more Ga are substituted into the system $E_g$ decreases reaching a value of 3.42 eV for 5% Ga doping. According to Vagard's law, since $Ga_2O_3$ has a larger band (4.9 eV) than ZnO, $E_g$ for the $Zn_{1-x}Ga_xO$ system should linearly increase with increase in Ga doping concentration.

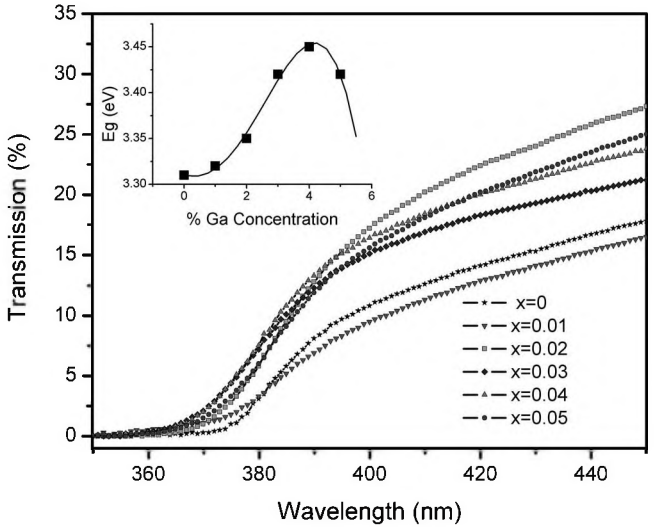


FIG. 6. Optical transmission scans over the wavelength range of 350–450 nm for the $Zn_{1-x}Ga_xO$ ($x$=0–0.05) samples. The inset shows the variation in $E_g$ with Ga concentration.

However, there are additional consequences of Ga doping that may effect $E_g$ such as increased electron doping and lattice distortion. In epitaxial thin films we showed a similar trend in $E_g$ with increased Ga doping.[17] In this case the contraction of $E_g$ at high Ga concentration was understood to be due to strong electron correlation that resulted in deformation of the band structure.

The experimentally recorded Raman data for the $Zn_{1-x}Ga_xO$ samples along with those of the ZnO precursor sample are shown in Fig. 7. Wurtzite ZnO belongs to the $C_{6v}^4$ ($P6_3mc$) space group, which according to theoretical group analysis has eight optical modes that exist at the $\Gamma$ point of the Brillouin zone, $\Gamma=A_1(\mathrm{TO},\mathrm{LO})+2B_1+E_1(\mathrm{TO},\mathrm{LO})+2E_2$.[18] Of the eight optic modes the two $B_1$ modes are silent and the $A_1$, $E_1$, and $E_2$ are Raman active. Because ZnO is polar along the $c$ axis of its hexagonal unit cell, which is caused by alternating layers of $Zn^{2+}$ and $O^{2-}$ ions, the $A_1$ and $E_1$ modes further split into transverse and longitudinal components. This accounts for four of the six active modes. The remaining two modes come from low and high frequency submodes of $E_2$, which are commonly designated as $E_2^{(1)}$ and $E_2^{(2)}$, respectively. In the Raman spectrum for the ZnO precursor sample, we observe five distinct peaks at 383, 410, 437.2, 539.9, and 582 $cm^{-1}$ corresponding to $A_1(\mathrm{TO})$, $E_1(\mathrm{TO})$, $E_2^{(2)}$, $A_1(\mathrm{LO})$, and $E_1(\mathrm{LO})$ modes, respectively. Upon comparison of the ZnO sol-gel and precursor samples it can be seen that their Raman spectra are quite similar, apart from the fact that the sol-gel sample peaks are much less intense and broader. The remaining five spectra are somewhat different from the two pure ZnO samples. They still retain the $A_1(\mathrm{TO})$ and $E_1(\mathrm{TO})$ modes, but the $A_1(\mathrm{TO})$ mode steadily loses intensity as Ga doping increases and the $E_1(\mathrm{TO})$ mode becomes more intense. We also see the appearance of three new modes at 512, 594, and 639 $cm^{-1}$ in the Ga doped samples. The mode at 594 $cm^{-1}$ is sensitive to Ga concentration and continuously increases with increasing Ga concentration.

In the Raman spectrum of ZnO the $E_2^{(2)}$ peak is associated with high sample crystallinity while the $E_1(\mathrm{TO})$ peak is associated with the existence of sample defects.[4] Therefore,

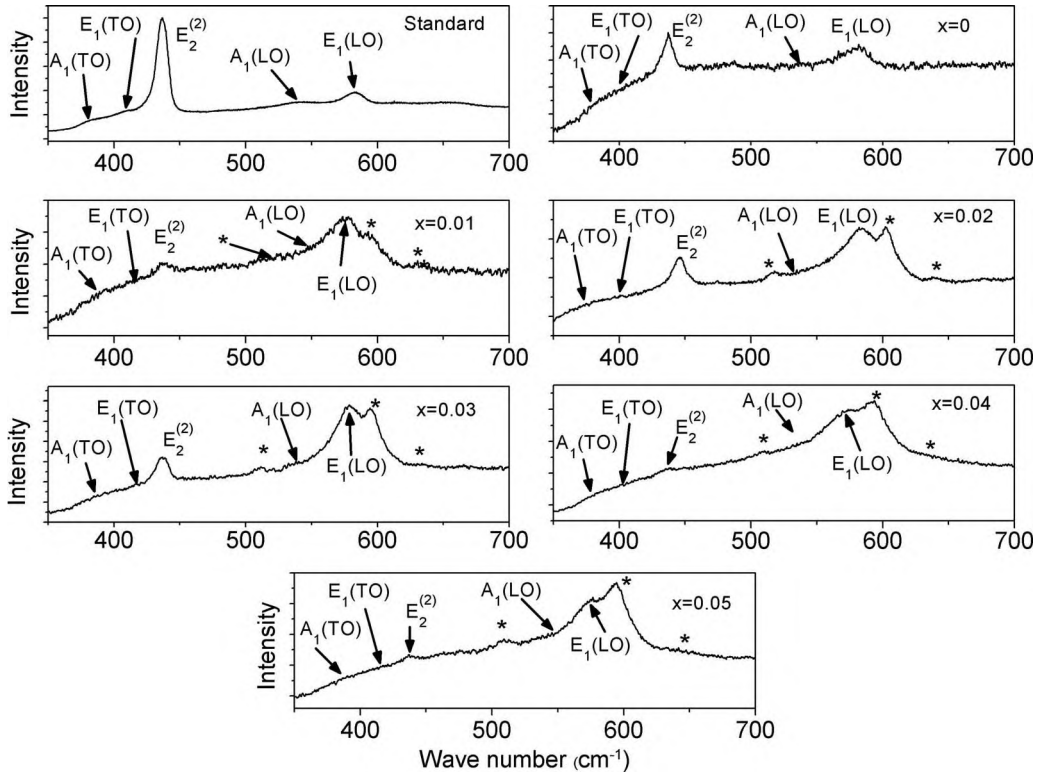


FIG. 7. Raman spectrum for the $Zn_{1-x}Ga_xO$ nanopowders. For comparison we have also shown the Raman data for the coarse ZnO precursor powder. Peaks marked with "*" represent additional modes not observed in the pure ZnO sample.

the $E_2^{(2)}/E_1(\mathrm{TO})$ ratio is a good indication of how crystalline the samples are. As can be clearly seen in Fig. 7, the $E_2^{(2)}/E_1(\mathrm{TO})$ ratio is considerably smaller in sol-gel samples as compared to the precursor material. This is consistent with the nanocrystalline nature of the material as observed in SEM and XRD data. The appearance of additional modes in the Ga doped samples is also consistent with previous experimental results on Ga doped ZnO thin films.[19,20] These modes appear due to the differences in mass and ionic radii between Ga and the host Zn atoms. These differences create defects in the host lattice, which may activate new modes and may also enhance soft modes that were not previously detectable.

## IV. CONCLUSION

In summary, single phase nanostructured $Zn_{1-x}Ga_xO$ ($x=0-0.05$) powders were synthesized using a low temperature solution-based technique. The structural and optical properties of the nanopowders were examined and compared with those of the coarse ZnO sample. As the Ga concentration was increased in the system, we saw an expansion in the lattice volume until a maximum was reached at 3% Ga. This was followed by a contraction in the lattice volume upon further Ga doping. PL showed a strong redshift in the emission due to the formation of deep level traps and revealed that Ga doping results in new emission peaks in blue and violet portions of the spectrum. Additionally, Ga doping causes an initial expansion in the band gap of the material with a maximum band gap value of 3.42 eV for the $Zn_{0.96}Ga_{0.04}O$ sample. Raman spectroscopic investigations showed that the doping of Ga not only changes the optical properties of ZnO but also perturbs the host lattice, which results in the creation of new vibrational modes.

## ACKNOWLEDGMENTS

The authors want to thank National Science Foundation (Contract No. DMR-0746486) for their financial support.

[1] S. J. Pearton, D. P. Norton, K. Ip, Y. W. Heo, and T. Steiner, Prog. Mater. Sci. **50**, 293 (2005).
[2] L. Kukreja, S. Barik, and P. Misra, J. Cryst. Growth **268**, 531 (2004).
[3] C. Teng, J. Muth, U. Ozgur, M. Bergmann, H. Everitt, A. Sharma, C. Jin, and J. Narayan, Appl. Phys. Lett. **76**, 979 (2000).
[4] A. Tiwari, M. Park, C. Jin, H. wang, D. Kumar, and J. Narayan, J. Mater. Res. **17**, 2480 (2002).
[5] K. Vanheusden, W. L. Warren, C. H. Seager, D. R. Tallant, J. A. Voigt, and B. E. Gnade, J. Appl. Phys. **79**, 7983 (1996).
[6] H. Angerer, D. Brunner, F. Freudenberg, O. Ambacher, M. Stutzmann, R. Hopler, T. Metzger, E. Born, G. Dollinger, A. Bergmaier, S. Karsch, and H. J. Korner, Appl. Phys. Lett. **71**, 1504 (1997).
[7] S. C. Jain, M. Willander, J. Narayan, and R. Van Overstraeten, J. Appl. Phys. **87**, 965 (2000).
[8] A. Tiwari, C. Jin, A. Kvit, D. Kumar, J. F. Muth, and J. Narayan, Solid State Commun. **121**, 371 (2002).
[9] X. Kong, Y. Ding, R. Yang, and Z. Wang, Science **303**, 1348 (2004).
[10] P. Gao, Y. Ding, W. Mai, W. Hughes, C. Lao, and Z. Wang, Science **309**, 1700 (2005).
[11] M. Snure and A. Tiwari, J. Nanosci. Nanotechnol. **7**, 481 (2007).
[12] B. Cullity and S. Stock, *Elements of X-ray Diffraction* (Prentice-Hall, Englewood Cliffs, NJ, 2001), p. 170.
[13] M. Leszczynski, H. Teisseyre, T. Suki, I. Grzegory, M. Bockowski, J. Jun, S. Porowski, K. Pakula, J. Baranowski, C. Foxon, and T. Cheng, Appl. Phys. Lett. **69**, 73 (1996).
[14] M. Leszczynski, J. Bak-Misiuk, J. Domagala, J. Muszalski, M. Kaniewska, and J. Marczewski, Appl. Phys. Lett. **67**, 539 (1995).
[15] Y. Lin, J. Xie, H. Wang, Y. Li, C. Chavez, S. Lee, S. Fottyn, S. Crooker, A. Burrell, T. McCleskey, and Q. Jia, Thin Solid Films **492**, 8 (2002).
[16] S. Studenikin and M. Cocivera, J. Appl. Phys. **91**, 5060 (2002).
[17] M. Snure and A. Tiwari, J. Appl. Phys. **101**, 124912 (2007).
[18] A. Tiwari, C. Jin, J. Narayan, and M. Park, J. Appl. Phys. **96**, 3827 (2004).
[19] C. Bundesmann, N. Ashkenov, M. Schubert, D. Spemann, T. Butz, E. M. Kaidashev, M. Lorenz, and M. Grundmann, Appl. Phys. Lett. **83**, 1974 (2003).
[20] A. Kaschner, U. Haboeck, M. Strassburg, M. Strassburg, G. Kaczmarczyk, A. Hoffmann, C. Thomsen, A. Zeuner, H. R. Alves, D. M. Hofmann, and B. K. Meyer, Appl. Phys. Lett. **80**, 1909 (2002).